Phosphatidylinositol 4,5-bisphosphate regulates inspiratory burst activity in the neonatal mouse preBötzinger complex

Erin A. Crowder[1], Margaret S. Saha[2], Ryland W. Pace[1], Honglu Zhang[3], Glenn D. Prestwich[3] and Christopher A. Del Negro[1]

[1]*Department of Applied Science, McGlothlin-Street Hall and* [2]*Department of Biology, Millington Hall, The College of William and Mary, Williamsburg, VA 23187-8795, USA*

[3]*Department of Medicinal Chemistry, The University of Utah, 419 Wakara Way Suite 205, Salt Lake City, UT 84108, USA*

Neurons of the preBötzinger complex (preBötC) form local excitatory networks and synchronously discharge bursts of action potentials during the inspiratory phase of respiratory network activity. Synaptic input periodically evokes a Ca^{2+}-activated non-specific cation current (I_{CAN}) postsynaptically to generate 10–30 mV transient depolarizations, dubbed inspiratory drive potentials, which underlie inspiratory bursts. The molecular identity of I_{CAN} and its regulation by intracellular signalling mechanisms during inspiratory drive potential generation remains unknown. Here we show that mRNAs coding for two members of the transient receptor potential (TRP) family of ion channels, namely TRPM4 and TRPM5, are expressed within the preBötC region of neonatal mice. Hypothesizing that the phosphoinositides maintaining TRPM4 and TRPM5 channel sensitivity to Ca^{2+} may similarly influence I_{CAN} and thus regulate inspiratory drive potentials, we manipulated intracellular phosphatidylinositol 4,5-bisphosphate (PIP_2) and measured its effect on preBötC neurons in the context of ongoing respiratory-related rhythms in slice preparations. Consistent with the involvement of TRPM4 and TRPM5, excess PIP_2 augmented the inspiratory drive potential and diminution of PIP_2 reduced it; sensitivity to flufenamic acid (FFA) suggested that these effects of PIP_2 were I_{CAN} mediated. Inositol 1,4,5-trisphosphate (IP_3), the product of PIP_2 hydrolysis, ordinarily causes IP_3 receptor-mediated I_{CAN} activation. Simultaneously increasing PIP_2 while blocking IP_3 receptors intracellularly counteracted the reduction in the inspiratory drive potential that normally resulted from IP_3 receptor blockade. We propose that PIP_2 protects I_{CAN} from rundown by interacting directly with underlying ion channels and preventing desensitization, which may enhance the robustness of respiratory rhythm.

(Received 13 April 2007; accepted after revision 21 June 2007; first published online 28 June 2007)
Corresponding author C. A. Del Negro: Department of Applied Science, McGlothlin-Street Hall, The College of William and Mary, Williamsburg, VA 23187-8795. Email: cadeln@wm.edu

Rhythmically active networks throughout the CNS generate activity patterns ranging from locomotor bursts (< 1 Hz) to gamma voltage oscillations (30–90 Hz) (Buzsáki, 2006). The characteristic features of these rhythms can often be attributed to specific ion channels and intracellular regulatory mechanisms that control the voltage trajectories of the constituent neurons and ultimately govern the form of the network output (Grillner, 2003, 2006; Bartos *et al.* 2007).

Breathing is a particularly important rhythmic behaviour in mammals that originates in the brainstem. Neurons within the ventral medullary site dubbed the preBötzinger complex (preBötC) synchronously discharge bursts of action potentials and drive inspiratory breathing movements (Smith *et al.* 1991; Rekling & Feldman, 1998; Feldman & Del Negro, 2006; Janczewski & Feldman, 2006). Although the rhythmogenic role of the preBötC is generally well accepted, the molecular mechanisms and intracellular signalling pathways that regulate inspiratory burst generation in preBötC neurons are not entirely clear.

Calcium-activated non-specific cation current (I_{CAN}) contributes postsynaptically to inspiratory burst generation (Pace *et al.* 2007*a*). The ion channel(s) underlying I_{CAN} may belong to the *transient receptor potential* (TRP) family of ion channels first identified in *Drosophila*

This paper has online supplemental material.

 DOI: 10.1113/jphysiol.2007.134577

(Minke, 1977). Members of the melastatin-like subfamily TRPM4 and TRPM5 are unique among TRP channels because they form flufenamic acid (FFA)-sensitive, Ca^{2+}-impermeable monovalent cation channels gated by intracellular Ca^{2+} transients (Launay *et al.* 2002; Hofmann *et al.* 2003; Montell, 2005; Ullrich *et al.* 2005; Ramsey *et al.* 2006), which are properties expressed by I_{CAN} at the whole-cell level in a variety of cell types (Teulon, 2000) including preBötC neurons (Pace *et al.* 2007*a*). If TRPM4 and TRPM5 give rise to I_{CAN} in preBötC neurons, then their regulation could influence I_{CAN} on a cycle-to-cycle basis and thus shape inspiratory bursts during respiratory rhythm generation.

The function of TRPM4 and TRPM5 is intimately coupled to phosphoinositide signalling (Fig. 1). For example, phosphatidylinositol 4,5-bisphosphate (PIP_2) maintains the Ca^{2+} sensitivity required to activate TRPM4 and TRPM5 channels (Liu & Liman, 2003; Zhang *et al.* 2005; Nilius *et al.* 2006) and thus PIP_2 depletion leads to TRPM4 and TRPM5 desensitization (Liu & Liman, 2003; Nilius *et al.* 2006). Phosphoinositide (PI) signalling also evokes TRPM4 and TRPM5 channel currents (as well as I_{CAN}) because PIP_2 hydrolysis forms inositol 1,4,5-trisphosphate (IP_3) and causes IP_3 receptor-mediated intracellular Ca^{2+} release (Clapham, 2003; Hofmann *et al.* 2003), which is important for inspiratory bursts in preBötC neurons (Pace *et al.* 2007*a*). If TRPM4 and TRPM5 underlie I_{CAN}, then the cycling of PIP_2 and IP_3 could provide feedback mechanisms that regulate drive potential generation. PIP_2 hydrolysis should deplete PIP_2 stores and ultimately lead to TRPM4 and TRPM5 channel desensitization. Thus, determining how PI signalling regulates I_{CAN} may be important to understand how respiratory rhythm, which must function unceasingly to sustain breathing, remains robust and stable.

Based on the likelihood that TRPM4 and TRPM5 channels give rise to I_{CAN}, here we test the two-part hypothesis that TRPM4 and TRPM5 channels are expressed within the preBötC region and that PIP_2 regulates inspiratory burst generation. By limiting I_{CAN} desensitization, we propose that PIP_2 promotes periodic recruitment of I_{CAN} and prevents the rundown of its inspiratory burst-generating function in preBötC neurons, which may help maintain robust breathing rhythms.

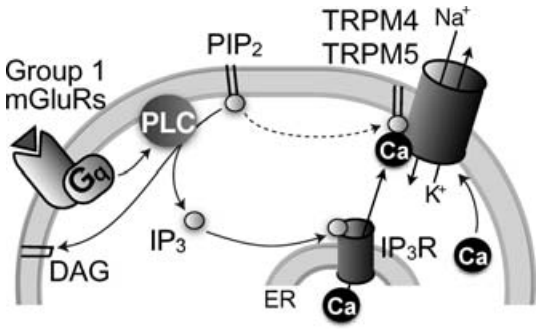

Figure 1. Model of I_{CAN} activation with hypothesized channel identity and PIP_2 regulation
Glutamate (triangle) activates group 1 metabotropic glutamate receptors (mGluRs), which then cause G_q-proteins to stimulate phospholipase C (PLC). PLC hydrolyses PIP_2 into diacylgylcerol (DAG) and IP_3, which activates IP_3 receptors (IP_3R) causing Ca^{2+} release from the endoplasmic reticulum (ER). Intracellular Ca^{2+} gates TRPM4 and TRPM5 channels, causing Na^+ influx and K^+ efflux that results in depolarization from baseline membrane potentials of –60 mV. PIP_2 also acts directly on TRPM4 and TRPM5 channels to maintain Ca^{2+} sensitivity (dotted arrow).

Methods

Slice preparation

We used neonatal C57BL/6 mice (postnatal day 1–7 (P1–7)) for *in vitro* electrophysiology as well as RT-PCR experiments. The Institutional Animal Care and Use Committee at The College of William and Mary approved all protocols.

Neonatal mice were anaesthetized by hypothermia and rapidly decerebrated prior to dissection in normal artificial cerebrospinal fluid (ACSF) containing (mM): 124 NaCl, 3 KCl, 1.5 $CaCl_2$, 1 $MgSO_4$, 25 $NaHCO_3$, 0.5 NaH_2PO_4 and 30 D-glucose, equilibrated with 95% O_2 and 5% CO_2 with pH = 7.4. Transverse slices (550 μm thick) containing the preBötC as well as hypoglossal (XII) motoneurons and premotoneurons were sectioned using a vibrating microslicer. The rostral surface was cut just above the XII nerve roots at the level of the dorsomedial cell column and principal lateral loop of the inferior olivary nucleus; the preBötC was at or near the rostral surface (Gray *et al.* 1999; Ruangkittisakul *et al.* 2006). The caudal cut captured the obex.

Electrophysiology

Slices were placed rostral surface up in a 0.5 ml recording chamber on a fixed-stage microscope equipped with Koehler illumination and perfused with 27°C ACSF at 4 ml min^{-1}. ACSF K^+ concentration was raised to 9 mM and respiratory motor output was recorded from XII nerve roots using suction electrodes and a differential amplifier.

Differential interference contrast videomicroscopy (Inoue & Spring, 1997) was used to visualize neurons and control micropipette movements. Patch-clamp recordings were performed on neurons visualized in the preBötC region ventrally adjacent to the semi-compact division of the nucleus ambiguus (Gray *et al.* 1999; Wang *et al.* 2001; Ruangkittisakul *et al.* 2006). Inspiratory neurons discharge spikes superimposed upon a 200–500 ms envelope of depolarization dubbed the *inspiratory drive potential* that is coincident with XII discharge (Pace *et al.* 2007*a*,*b*). All

preBötC neurons with robust inspiratory activity were suitable for experiments; no attempt to identify neurons with voltage-dependent pacemaker properties was made and expiratory neurons were excluded. Current-clamp recordings were performed using a Dagan IX2-700 amplifier (Minneapolis, MN, USA). Intracellular pipettes were fabricated from capillary glass (O.D., 1.5 mm; I.D., 0.87 mm) and filled with patch solution (contents listed below). Access resistance was compensated with bridge balance. Data were digitally acquired at 4–20 kHz using a 16-bit A/D converter (Powerlab, ADInstruments, Colorado Springs, CO, USA) after low-pass filtering at 1 kHz to avoid aliasing.

We continuously monitored membrane potential and adjusted the bias current to maintain a consistent baseline of –60 mV, which provides a uniform standard for comparing inspiratory drive potentials among preBötC neurons. Inspiratory bursts were digitally smoothed to remove spikes and facilitate measurements of the underlying inspiratory drive potential (see Fig. 1 in Pace *et al.* 2007*b*) using Chart v5.4 (AD Instruments). The Peak Parameters extension in Chart software measured inspiratory drive potential amplitude and area.

The standard potassium gluconate patch solution contained (mM): 140 potassium gluconate, 5 NaCl, 1 EGTA, 10 Hepes, 2 Mg-ATP (excluded in some trials, e.g. Figs 3*B, D–F* and 5*B* and *C*) and 0.3 Na-GTP (pH = 7.3 with KOH). Pipette resistance was 3–4 MΩ and a liquid junction potential of 8 mV was corrected offline. One (or sometimes two, e.g. Fig. 5*B*) drugs that affect PIP_2 or IP_3 signalling pathways were added to the patch solution and applied intracellularly at the following concentrations: 10 μM PIP_2–1,2-dicotanoyl-sn-glycerol (diC8-PIP_2) (Echelon Biosciences, Salt Lake City, UT, USA), 30 μg ml^{-1} poly L-lysine (Sigma, St Louis, MO, USA), 50 μM wortmannin (Sigma), 1 μM Xestospongin-C (Sigma), or 10 μM PLC-resistant PIP_2 synthesized by H. Zhang and G. Prestwich (Zhang *et al.* 2006; analog 4).

Control measurements of inspiratory drive potentials were obtained using nystatin-perforated patches. Nystatin (250 μg ml^{-1}) was added to potassium gluconate patch solution immediately prior to use and discarded after 120 min. The amplitude and area of the underlying inspiratory drive potentials could be accurately measured after ∼20 min of exposure to nystatin, even though the high impedance of the perforated patch partially attenuated action potentials (Pace *et al.* 2007*a*). Subsequently, drugs that target PIP_2 signalling pathways were delivered intracellularly via patch rupture, which dialyses the cytosol in the whole-cell configuration. Patch rupture also lowered access resistance and enabled action potentials to measure full amplitude. FFA (Sigma) was often bath-applied after intracellularly applied drugs achieved steady state.

The mean inspiratory drive potential and XII motor output were computed by averaging 10 consecutive inspiratory bursts. All samples were tested for normality using the Anderson–Darling test. Student's paired *t* tests and Wilcoxon signed ranks tests were applied to determine significance for normal and non-normal distributions, respectively, with minimum significance set at 0.05 or less. Experiments in which XII motor output changed significantly during the course of intracellular drug application were discarded.

RT-PCR

For reverse transcriptase polymerase chain reaction (RT-PCR) experiments, total RNA was purified from flash-frozen kidney tissue using RNeasy (Qiagen, Valencia, CA, USA). The preBötC kernel was dissected from bilateral regions of the slice preparation and immediately flash-frozen in liquid nitrogen. Total RNA from these samples was extracted with the RNaqueous Micro kit (Ambion, Austin, TX, USA). Possible genomic DNA contaminants were removed by incubating all RNA samples at 37°C with DNase (from RNAqueous kit or Promega, Madison, WI, USA) and either RNasin (Promega) or 1× Dnase I buffer (provided with RNAqueous kit). Using the iSCRIPT cDNA Synthesis kit (Bio-Rad, Hercules, CA, USA), cDNA was reverse transcribed from 1 μg of total RNA. Following the manufacturer's instructions, samples were incubated for 5 min at 25°C, 60 min at 42°C, and 5 min at 85°C. For negative controls, no reverse transcriptase was added to the reaction.

PCR was carried out using standard conditions: 0.5 μM of each primer, 1.5 mM $MgCl_2$, 0.2 mM deoxynucleoside triphosphates (dNTPs) and 1.25 U Supertaq polymerase (Ambion), although Supertaq buffer concentration was doubled (from 1×) for TRPM4 reactions to optimize the reaction. This conventional protocol was the basis for amplification: 5 min 94°C 'hot start' to prevent mis-priming, 40 cycles of 30 s at 94°C, 1–2 min primer annealing, and 1–2 min elongation at 72°C, followed by 7 min at 72°C, and finally holding at 4°C. These reaction conditions were modified as follows: TRPM4 reactions involved 1 min annealing at 60°C and 1 min elongation, TRPM5 reactions involved 2 min annealing at 57°C and 2 min elongation, and GADPH reactions involved 1 min annealing at 60°C and 2 min elongation. In order to assess the quality and presence of the cDNA, all samples were tested for a ubiquitously expressed gene, GADPH (accession no. NM_008084), using the following primers: Forward, 5′-ACCACAGTCCATGCCATCAC-3′; reverse, 5′-TCCACCACCCTGTTGCTGTA-3′ (Kunert-Keil *et al.* 2006). To test preBötC samples for the presence of TRPM4 (accession no. NM˙175130) and TRPM5

(accession no. NM_020277), the primer sets: forward, 5′-GGCCCAAGATTGTCATAGTG-3′; reverse, 5′-TTGGCATACTGGGACACACA-3′ (Guinamard *et al.* 2004*a*; note: forward and reverse primers were switched in this report); and forward, 5′-TCCTGTTCATTG-TGGGAGTCAC-3′; reverse, 5′-TGGCGATCAGAAGG-TTCATG-3′ (Paulsen *et al.* 2000), were used, respectively. All primers were designed to cross at least one intron as an additional control to assess the unintended amplification of residual genomic DNA; amplification of genomic DNA would result in a recognizably higher molecular weight fragment. Fragments amplified by each set of primers were verified via direct sequencing of PCR products using the ABI BigDye 3.1 kit (Applied Biosystems, Foster City, CA, USA) and ABI 3100-Avant automated fluorescent sequencer.

Results

TRPM4 and TRPM5 expression

We used RT-PCR to detect the presence of TRPM4 and TRPM5 mRNA in the preBotC. Murine kidney tissue expressing TRPM4 and TRPM5 mRNA (Enklaar *et al.* 2000; Nilius *et al.* 2003; Kunert-Keil *et al.* 2006) served as positive controls for both genes.

We dissected the preBötC region bilaterally from slice preparations. Following total RNA extraction, all preBötC samples ($n = 4$) tested positive for the presence of TRPM4, TRPM5 and GADPH mRNA, whereas mRNA for these genes was absent in negative controls (Fig. 2). Sequencing and comparison to the National Center for Biotechnology Information (NCBI) database confirmed the identity of all RT-PCR products, which indicates that cells in the preBötC region express mRNA for TRPM4 and TRPM5 ion channels. These data are consistent with the proposal that TRPM4 and/or TRPM5 give rise to I_{CAN} in preBötC neurons (Pace *et al.* 2007*a*).

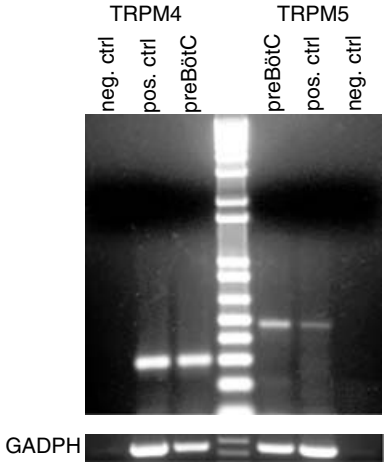

Figure 2. The mRNA coding for TRPM4 and TRPM5 is expressed in the preBötC region
Total RNA was extracted from preBötC and positive control tissues and reverse transcribed. Amplified products of the expected sizes were obtained for TRPM4 (301 bp), TRPM5 (483 bp) and GADPH (452 bp). Negative control reactions were performed without reverse transcriptase and amplified nothing.

It is important to note that this technique does not precisely quantify mRNA levels, but rather reliably detects only its presence or absence. For example, in many cases, taking a broad region of kidney tissue as a positive control diluted TRPM5 mRNA levels, so its band appeared weaker than the TRPM5 band for preBötC tissue (e.g. Fig. 2, compare TRPM5 preBötC to positive control). Intensity of bands should not be taken to indicate levels of expression, but rather the presence or absence of expression. Nevertheless, these data clearly demonstrate that TRPM4 and TRPM5 mRNA are present in the preBötC.

PIP_2 manipulation affects inspiratory burst generation in preBötC neurons

Synaptic excitation during the inspiratory phase involves metabotropic glutamate receptors (see Fig. 1) that stimulate IP_3 production and trigger intracellular Ca^{2+} release to evoke I_{CAN} (Pace *et al.* 2007*a*). In addition to its role as a precursor to IP_3, we posit that PIP_2 prevents I_{CAN} desensitization by regulating its Ca^{2+} sensitivity, because PIP_2 has this effect on TRPM4 and TRPM5 ion channels (Liu & Liman, 2003; Zhang *et al.* 2005; Nilius *et al.* 2006). Therefore, we predicted that augmenting the supply of PIP_2 intracellularly would promote I_{CAN} activation via increasing IP_3 production and simultaneously preventing desensitization; the net effect would be to enhance inspiratory drive potentials.

We increased the concentration of intracellular PIP_2 in a single inspiratory neuron using patch solution containing 10 μM of the water-soluble PIP_2 analogue diC8-PIP_2. The area and amplitude of the inspiratory drive potentials measured in control via perforated patch matched those observed during the first few cycles of whole-cell recording before diC8-PIP_2 dialysis occurred (e.g. Fig. 3*D* and *E*). Therefore, control inspiratory drive potentials may be measured either during perforated-patch conditions (with attenuated spikes) or from the first few cycles in whole cell (with spikes full amplitude). After 10 min of diC8-PIP_2 dialysis, inspiratory drive potential amplitude and area increased to $126 \pm 10\%$ and $203 \pm 16\%$ of control, respectively ($n = 3$).

Mg-ATP restores Ca^{2+} sensitivity to TRPM4 in excised patches (Nilius *et al.* 2005), in much the same way as PIP_2 (Nilius *et al.* 2006), and thus we could not differentiate whether diC8-PIP_2 or Mg-ATP caused drive potential enhancement. Therefore, we removed Mg-ATP from the

patch solution to isolate the putative effects of PIP_2 on I_{CAN} desensitization during inspiratory bursts and repeated the experiment.

As a control we removed Mg-ATP from the patch solution without adding diC8-PIP_2, which caused significant rundown in the inspiratory drive potential: amplitude and area decreased to 66 ± 12% and 58 ± 9% of control, respectively ($P < 0.05$, $n = 8$, Fig. 3*B*). In contrast, inspiratory drive potentials measured with potassium gluconate patch solution containing Mg-ATP did not change: amplitude and area were 100 ± 4% and 104 ± 6% of control, respectively ($P \gg 0.05$, $n = 6$, Fig. 3*C*). These data show that Mg-ATP prevents drive potential rundown but does not, on its own, enhance inspiratory drive potentials.

Dialysing preBötC neurons with diC8-PIP_2 in the absence of Mg-ATP nevertheless augmented inspiratory drive potentials: the amplitude and area significantly increased to 126 ± 7% and 177 ± 15% of perforated-patch control ($P < 0.05$, $n = 6$, Fig. 3*A*, *D* and *E*). Therefore,

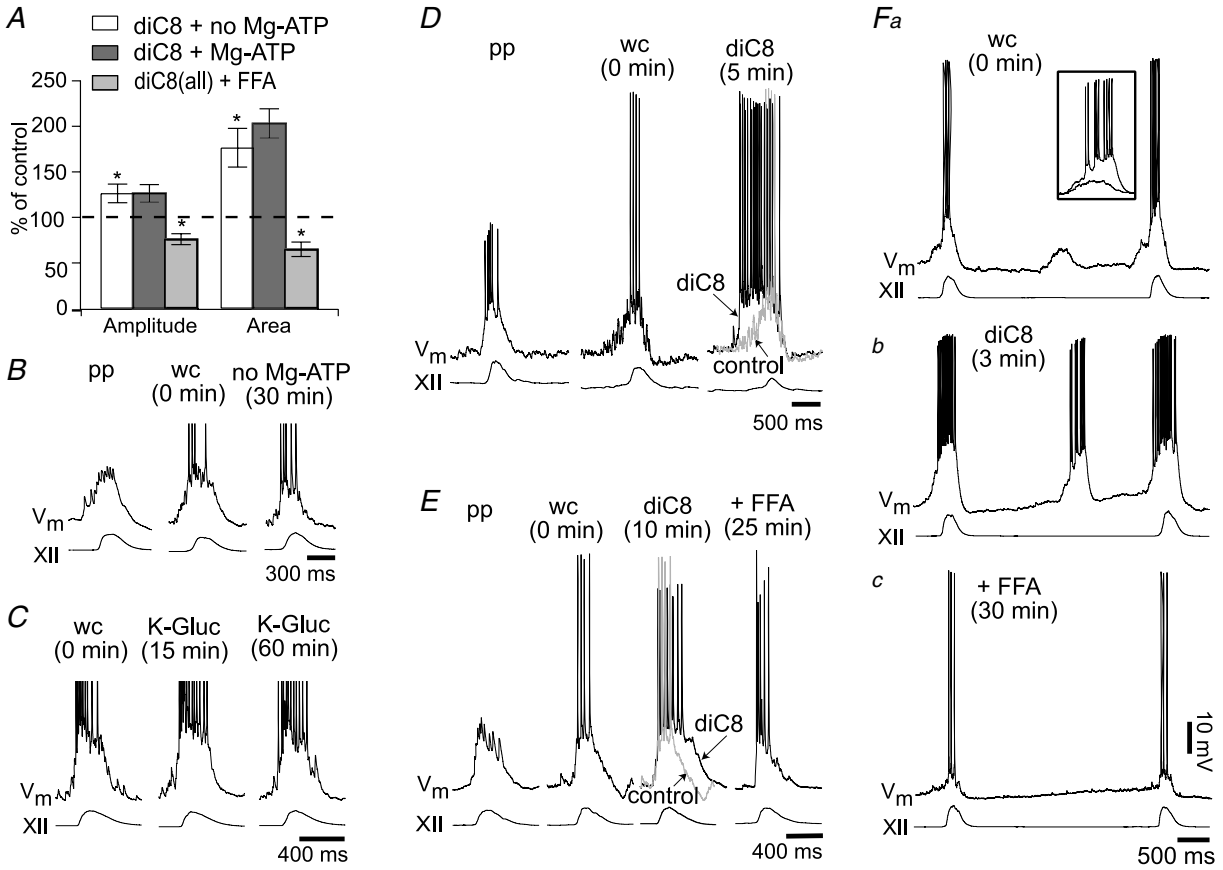

Figure 3. The effects of excess PIP_2 on inspiratory drive potentials
A, bar chart summarizing the effects of diC8-PIP_2 (diC8) on mean inspiratory drive potentials (± S.E.M.). Inspiratory drive potential amplitude and area are plotted as a per cent of control for the following conditions: 10 μM diC8 with Mg-ATP (dark grey bars) or diC8 without Mg-ATP (white bars). The same measure is shown for the effects of flufenamic acid (FFA, 100 μM) in the presence of diC8-PIP_2 (light grey bars). *Statistical significance at $P < 0.05$. *B*, representative traces showing the effects of Mg-ATP removal from the standard patch solution. Sequential traces represent perforated patch (pp), whole cell immediately after patch rupture (wc), and whole cell 30 min after patch rupture. Baseline membrane potential (V_m) was held at –60 mV. XII represents hypoglossal nerve motor output. Mg-ATP was excluded from all subsequent diC8 experiments in panels *D–F*. *C*, representative traces from a control experiment show drive potential stability and longevity under standard conditions *in vitro*. Standard patch solution was employed with Mg-ATP present. The drive potential did not change over 60 min. *D*, representative neuron showing diC8 enhancement of drive potential onset. Sequential traces show pp, wc and wc 5 min after diC8 dialysis. *E*, representative neuron showing diC8 prolongation of drive potentials and the effects of FFA. The sequence of traces are similar to *D* (above) with the additional FFA condition after 25 min of diC8 dialysis. *Fa–c*, the effects of diC8 and FFA on ectopic depolarizations in preBötC neurons. *Fa*, example of ectopic depolarizations observed immediately following patch rupture. Inset shows the superposition of ectopic depolarizations in control and diC8. *Fb*, the same cell 3 min after patch rupture. *Fc*, with diC8 still present, FFA was bath-applied and ectopic depolarizations disappeared entirely.

augmentation conferred by diC8-PIP_2 is an independent effect unrelated to Mg-ATP.

Of the six preBötC neurons dialysed with diC8-PIP_2 in the absence of Mg-ATP, four neurons activated more rapidly and attained maximum amplitude earlier during the inspiratory phase compared with control (Fig. 3*D*) whereas two neurons extended inspiratory burst duration (Fig. 3*E*). Three of the six exhibited spontaneous ectopic subthreshold depolarizations in the interval between XII discharge within the first minute of whole-cell recording (0 min, Fig. 3*Fa*) that were greatly enhanced by diC8-PIP_2 after reaching steady state ($= 3$ min, Fig. 3*Fb*). This enhancement of the ectopic burst is emphasized in the inset in Fig. 3*Fa*, which overlays the control and diC8-PIP_2 responses for comparison.

If the effects of diC8-PIP_2 are attributable to I_{CAN}, then they should be sensitive to the I_{CAN} antagonist FFA. In steady-state diC8-PIP_2 conditions, bath application of FFA reduced inspiratory drive potentials to below control levels: the amplitude and area decreased to $78 \pm 6\%$ and $68 \pm 7\%$ of control, respectively ($P < 0.05$, $n = 5$, e.g. Fig. 3*A*, *E* and *Fc*). These data are commensurate with the attenuation caused by bath-applied FFA in prior experiments that did not involve PIP_2 manipulations (65–70% of control (their Fig. 6), Pace *et al.* 2007*a*). The ability of FFA to reverse the burst-augmenting effects of diC8-PIP_2 indicates that I_{CAN} is the primary current affected by excess PIP_2.

Whereas excess PIP_2 enhanced inspiratory burst generation (Fig. 3), we next sought to test whether PIP_2 depletion would diminish the ability of preBötC neurons to generate inspiratory bursts (Fig. 4). We included Mg-ATP in the potassium gluconate patch solution so that any change in inspiratory drive potentials would be attributable to PIP_2 reduction, and not the removal of Mg-ATP (e.g. Fig. 3*C*).

Poly L-lysine (PLL) acts as a scavenger that reduces the amount of free PIP_2 in the plasma membrane (Suh & Hille, 2005) and attenuates TRPM4 currents in excised patches (Zhang *et al.* 2005; Nilius *et al.* 2006). Applied to preBötC neurons intracellularly with Mg-ATP present, 30 μg ml^{-1} PLL significantly decreased inspiratory drive potential amplitude and area to $79 \pm 6\%$ and $70 \pm 7\%$ of perforated-patch control (amplitude $P < 0.05$, area $P < 0.01$, $n = 7$); a representative experiment is shown in Fig. 4*A*. Subsequent FFA application significantly reduced the amplitude and area of inspiratory drive potentials to $65 \pm 7\%$ and $36 \pm 7\%$ of control ($P < 0.01$, $n = 7$, Fig. 4*A*). These data suggest that PIP_2 depletion diminishes PI-sensitive mechanisms that contribute to drive potential generation, including (but not limited to) I_{CAN}. PLL scavenging does not completely block I_{CAN} because the effects of FFA were not occluded.

As a complementary experiment, we depleted PIP_2 using wortmannin, an inhibitor of PI 4-kinase that hinders PIP_2 production by preventing the synthesis

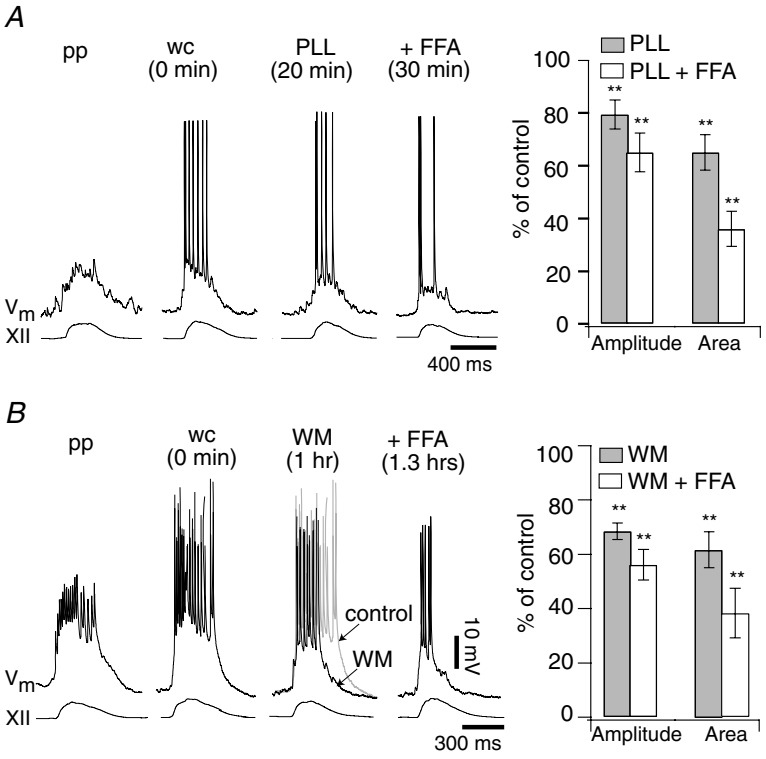

Figure 4. The effects of PIP_2 removal on inspiratory drive potentials
A, sequential traces show the response of a representative inspiratory neuron to intracellular 30 μg ml^{-1} poly L-lysine (PLL) and FFA. Perforated patch (pp) and whole cell immediately following patch rupture (wc) represent controls. PLL reached steady state after 20 min of whole-cell dialysis. Then, FFA was applied; the illustrated trace was taken at 30 min. The bar graph plots the mean drive potential amplitude and area (± S.E.M.) as per cent of control in response to PLL applied alone (grey bars) and in combination with FFA (white bars). *B*, sequential traces show the effects of intracellular application of 50 μM wortmannin (WM) and FFA on a representative inspiratory neuron. The control trace is superimposed (in grey) on top of the WM trace for comparison. The bar graph plots the mean drive potential amplitude and area (± S.E.M.) as per cent of control after application of WM alone (grey bars) and co-application of WM and FFA (white bars). For both graphs, ** denote statistical significance at $P < 0.01$ compared with pp or wc control.

of its precursor phosphatidylinositol 4-monophosphate from PI (Nakanishi *et al.* 1995) and causes TRPM4 channel desensitization (Zhang *et al.* 2005; Nilius *et al.* 2006). Applied intracellularly with Mg-ATP in the patch solution and a perforated-patch control, 50 μM wortmannin significantly decreased inspiratory drive potential amplitude and area to $65 \pm 4\%$ and $61 \pm 6\%$ of control, respectively ($P < 0.01$, $n = 8$, Fig. 4*B*). FFA application further attenuated inspiratory drive potential amplitude and area to $56 \pm 6\%$ and $38 \pm 11\%$ of control ($P < 0.01$, $n = 7$, Fig. 4*B*). These data suggest that inhibiting the synthesis of PIP_2 reduces the inspiratory burst-generating capabilities of preBötC neurons. However, wortmannin does not completely block the FFA-sensitive intrinsic current consistent with I_{CAN}, similar to an analogous experiment with PLL.

We showed that excess PIP_2 augments inspiratory drive potentials and that diminution of PIP_2 attenuates them. However, these effects may be explained in several ways. For example, PIP_2 may affect I_{CAN} by promoting IP_3-mediated Ca^{2+} release and I_{CAN} activation, or by interacting directly with the underlying channels to affect sensitivity to Ca^{2+}, or through some combination of both pathways (Fig. 1). Additionally, excess PIP_2 may increase diacylglycerol (DAG) levels, which regulates TRPM4 in cardiac myocytes (Guinamard *et al.* 2004*a*,*b*). Therefore, we designed experiments to differentiate the PIP_2-mediated effects on I_{CAN} desensitization from IP_3- and DAG-dependent I_{CAN} activation.

IP_3 receptor-mediated I_{CAN} activation is prevented by intracellularly applying the IP_3 receptor antagonist Xestospongin-C (Xes; 1 μM) (Gafni *et al.* 1997). In a prior study we reported that Xes reduced inspiratory drive potential amplitude and area to $67 \pm 5\%$ and $64 \pm 6\%$ of perforated-patch control ($P < 0.01$, $n = 16$) by acting to prevent IP_3-mediated Ca^{2+} release involved in I_{CAN} activation (Pace *et al.* 2007*a*). Original data are shown in Fig. 5*A*.

To test directly the role of PIP_2 in I_{CAN} desensitization, we coupled intracellular dialysis of diC8-PIP_2 with Xes (in the absence of Mg-ATP) to prevent IP_3 receptor-mediated Ca^{2+} release. If exogenous PIP_2 acts exclusively through the IP_3 pathway, and not by preventing I_{CAN} desensitization, then Xes should still attenuate inspiratory drive potentials, even in the presence of excess PIP_2 (see Fig. 5*D* (white bars) and Pace *et al.* 2007*a*). However, the combined dialysis of Xes and diC8-PIP_2 caused no statistically significant change compared with perforated-patch control (Fig. 5*B*): inspiratory drive potential amplitude and area measured $110 \pm 8\%$ and $130 \pm 14\%$ of control, respectively ($P >> 0.05$, $n = 10$, Fig. 5*D*, dark grey bars). These results suggest that the effects of excess PIP_2 (i.e. to augment inspiratory drive potentials as shown in Fig. 3*A* and *D–F*) are not solely attributable to increased IP_3 levels.

The protocol in Fig. 5*B* tests the direct effects of PIP_2 on I_{CAN} desensitization but does not preclude DAG signalling since Xes only blocks IP_3 receptors. Our subsequent test (Fig. 5*C*) precludes both IP_3 and DAG

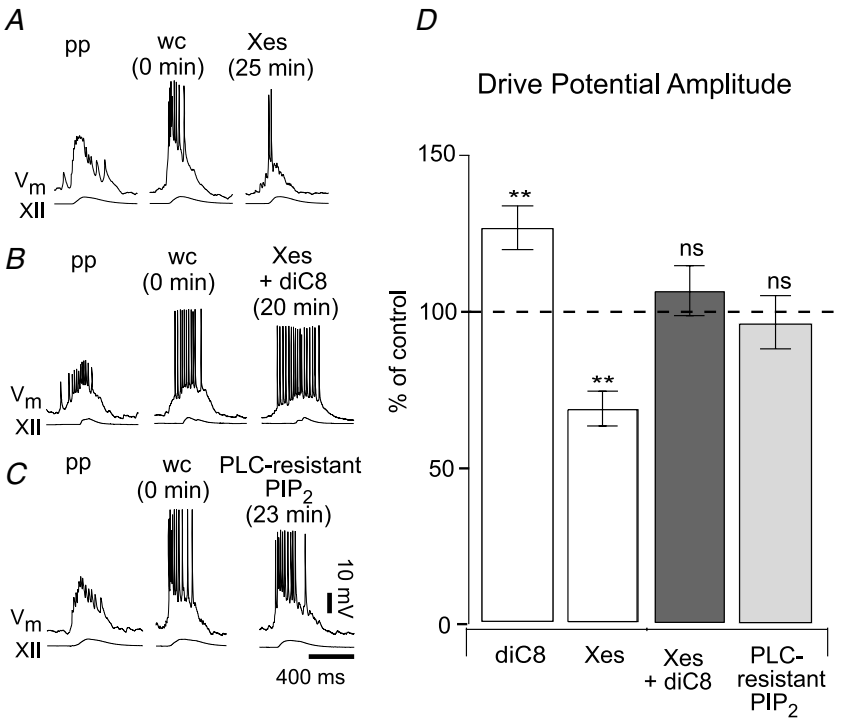

Figure 5. Excess PIP_2 augments drive potentials through an IP_3-independent mechanism
A, intracellular Xestospongin (Xes, 1 μM) attenuates inspiratory drive potentials by blocking IP_3 receptors. Perforated-patch (pp) and whole-cell (wc) control conditions are illustrated along with whole-cell Xes dialysis at steady state. *B*, typical data from an inspiratory neuron in response to co-application of Xes and diC8-PIP_2 (diC8). The inspiratory burst changed shape somewhat but neither amplitude nor area changed significantly. *C*, typical response to 10 μM intracellular PLC-resistant PIP_2. Again, neither the amplitude nor the area of the inspiratory burst changed significantly. *D*, bar chart plots the mean amplitude of inspiratory drive potentials (± S.E.M.) as per cent of control in the following conditions: diC8 alone (left white bar), Xes alone (right white bar), co-applied diC8 and Xes (dark grey bar), and PLC-resistant PIP_2 (light grey bar). Here ** denotes $P < 0.01$ and ns denotes 'not significant' at $P \gg 0.05$.

production. We intracellularly dialysed preBötC neurons with a water-soluble PIP_2 analogue that lacks the scissile P–O bond normally cleaved by PLC and thus cannot be hydrolysed into IP_3 and DAG. This PLC-resistant PIP_2 at high intracellular concentrations functions normally in maintaining Ca^{2+} sensitivity of TRPM4 (Zhang *et al.* 2006), and is predicted to outcompete with endogenous PIP_2 for PLC binding sites (W. Huang and G. D. Prestwich, unpublished molecular simulations) and thus occlude IP_3-dependent I_{CAN} activation by preventing IP_3 synthesis. Finally, if DAG does not contribute to the diC8-PIP_2 effects, then we predict commensurate results between PLC-resistant PIP_2 and co-application of Xes with diC8-PIP_2 (e.g. Fig. 5*B*).

The PLC-resistant PIP_2 (10 μM) caused no significant change in the inspiratory drive potential amplitude or area compared with perforated-patch control; these measures remained at $95 \pm 8\%$ and $97 \pm 9\%$ of control, respectively ($P \gg 0.05$, $n = 8$). Figure 5*C* shows a representative experiment; mean data for amplitude are shown in part D. These data are consistent with PIP_2 directly influencing the Ca^{2+} sensitivity of I_{CAN}.

Discussion

Here we demonstrate that PIP_2 directly regulates inspiratory drive potentials during endogenous respiratory-related rhythmic activity. We propose that PIP_2 prevents long-term desensitization of I_{CAN} through interactions with underlying TRPM4 and TRPM5 channels.

Experimental approach to study I_{CAN} regulation in the context of inspiratory bursts

PIP_2 regulates TRPM4 and TRPM5 ion channels that give rise to I_{CAN}-like whole-cell currents (Liu & Liman, 2003; Zhang *et al.* 2005; Nilius *et al.* 2006). We now show that manipulating PIP_2 can both enhance as well as diminish inspiratory drive potentials in the context of endogenous respiratory-related behaviour *in vitro*.

Our objective is to understand the mechanisms that regulate inspiratory bursts, so we cannot study I_{CAN} using excised patch or whole-cell experiments from cell lines expressing only TRPM4 or TRPM5 ion channels. These experimental approaches are divorced from respiratory function *in vitro*. In addition, excised patch (Liu & Liman, 2003; Zhang *et al.* 2005; Nilius *et al.* 2006) and Ca^{2+} uncaging experiments (Ullrich *et al.* 2005) employ Ca^{2+} concentrations of 1 μM to 10 mM to evoke TRPM4 and TRPM5 currents, which may exaggerate Ca^{2+}-dependent rundown of channel activity (Liu & Liman, 2003; Nilius *et al.* 2004). We do not yet know how these experimentally induced Ca^{2+} levels compare to the physiologically relevant Ca^{2+} fluctuations in preBötC neurons. Therefore we aimed to study PI regulation of inspiratory drive potentials, and by inference the role of I_{CAN} desensitization, with the endogenous preBötC rhythm intact.

I_{CAN} is the major charge carrier of the drive potential (Pace *et al.* 2007*a*), but it is not the only contributor pre- or postsynaptically. We used 100 μM FFA to ensure that our PIP_2 manipulations modified drive potentials via effects on I_{CAN} and not other intrinsic currents that contribute to drive potentials. FFA (100 μM) significantly attenuates I_{CAN} (Pace *et al.* 2007*a*). In various other neurons, this dose of FFA also affects: (i) gap junctions, (ii) NMDA receptors, (iii) Ca^{2+}-activated Cl^- channels, and (iv) Ca^{2+}-dependent K^+ currents ($I_{K\text{-}Ca}$) (Ottolia & Toro, 1994; Greenwood & Large, 1995; Teulon, 2000; Harks *et al.* 2001; Srinivas & Spray, 2003; Wang *et al.* 2006). However, in preBötC neurons, 100 μM FFA had no effect on inspiratory drive potentials following intracellular blockade of I_{CAN} accomplished with the rapid intracellular Ca^{2+} buffer BAPTA (Pace *et al.* 2007*a*). These results indicate that the first three FFA side-effects (listed above) do not significantly influence inspiratory drive potential properties, and thus do not confound our use of FFA to test for the involvement of I_{CAN} in the current study.

We do not yet know whether FFA affects $I_{K\text{-}Ca}$ in preBötC neurons (cf. Wang *et al.* 2006). Ca^{2+}-dependent K^+ currents contribute to burst termination in adult mammals, as shown in cats *in vivo* (Richter *et al.* 1993; Pierrefiche *et al.* 1995), but $I_{K\text{-}Ca}$ does not significantly contribute to inspiratory drive potentials in preBötC neurons of neonatal mice (see Supplementary Fig. 1). Therefore, even if 100 μM FFA affects $I_{K\text{-}Ca}$, this side-effect would not be relevant to the periodic regulation of inspiratory drive potentials.

PIP_2 regulation of inspiratory drive potentials probably involves I_{CAN}

If excess PIP_2 augments drive potentials by enhancing I_{CAN}, then the I_{CAN} antagonist FFA should be equally effective if applied with diC8-PIP_2 as when applied alone. The combined application of diC8-PIP_2 and FFA decreased drive potentials to 65–75% of control; this is the same level of attenuation reported by Pace *et al.* (2007*a*) in experiments where FFA was applied alone. We conclude that excess intracellular PIP_2 enhances the burst-generating contribution of I_{CAN}.

Conversely, if PIP_2 removal acts principally to diminish I_{CAN}, then drive potential amplitude and area should decline in the presence of PLL or wortmannin, which we observed. One might predict that the inspiratory burst-generating role of I_{CAN} in preBötC neurons would be abolished entirely during PLL or wortmannin trials because the absence of PIP_2 has been shown to completely

block TRPM4 and TRPM5 channel currents (Liu & Liman, 2003; Zhang *et al.* 2005; Nilius *et al.* 2006). However, the presence of Mg-ATP prevents complete TRPM4 channel desensitization after PIP_2 removal (Zhang *et al.* 2005), which is probably attributable to the necessary role of Mg-ATP in maintaining PI 4-kinases (Balla, 1998). Based on these findings, we expect a fraction of I_{CAN} in preBötC neurons to remain available following PIP_2 depletion and thus able to activate in response to intracellular Ca^{2+} attributable to NMDA receptor- or Ca^{2+} channel-mediated fluxes.

However, we are left with the conundrum that co-application of FFA with PLL or wortmannin decreased inspiratory drive potentials to a greater extent (area measured ∼36% of control, see Fig. 4) than FFA alone (∼65% of control, see Pace *et al.* 2007*a*). This suggests that PIP_2 removal might decrease the drive potential by affecting synaptic and intrinsic currents other than I_{CAN}, that are also sensitive to PIP_2 levels.

PIP_2 promotes activation of several ion channel types including HCN, TRPM7 and TRPM8 (Runnels *et al.* 2002; Rohacs *et al.* 2005; Suh & Hille, 2005; Zolles *et al.* 2006) so we cannot rule out the possibility that PIP_2 removal influences the burst-generating function of preBötC neurons via effects on multiple intrinsic membrane properties besides I_{CAN}. However, HCN channels that underlie the mixed cationic current I_h appear to influence respiratory frequency but not inspiratory burst generation (Mironov *et al.* 2000; Thoby-Brisson *et al.* 2000). It is currently unknown whether TRPM7 and/or TRPM8 channels are expressed in preBötC neurons and is beyond the scope of the present investigation. In addition, PIP_2 might be required for mGluR1-mediated mechanisms of inspiratory drive potential generation that involve K^+ currents, not I_{CAN} (Pace *et al.* 2007*a*).

Furthermore, PLL and wortmannin undoubtedly cause rundown of intrinsic currents that depend on PKC phosphorylation because PIP_2 hydrolysis produces DAG, which in turn activates protein kinase C (PKC) (Hille, 2001). However, since the hydrolysable compound diC8-PIP_2 in the presence of Xes compared with the PLC-resistant PIP_2 analogue yielded similar results, we concluded that DAG is not a major factor in drive potential generation.

In addition to group I mGluRs, other important metabotropic receptors in preBötC neurons, including neurokinin 1 receptors (NK1Rs) and subtype 1 of the purinergic P2Y receptors ($P2Y_1R$) may activate the PLC pathway via G_q-protein and therefore utilize PIP_2 (Li *et al.* 1997; North & Barnard, 1997). However, the signalling pathways underlying NK1R and $P2Y_1R$ actions in preBötC neurons remain to be determined; for example, NK1Rs can be coupled to a wide variety of G-proteins (Roush & Kwatra, 1998). Moreover, previous studies have shown that NK1Rs and $P2Y_1Rs$ primarily regulate respiratory frequency (Gray *et al.* 1999; Pena & Ramirez, 2004; Lorier *et al.* 2007). In contrast, inspiratory drive potentials depend on metabotropic glutamate receptors coupled to PLC signalling, and this process is largely independent of frequency modulation (Pace *et al.* 2007*a*). Nevertheless, $P2Y_1R$ and NK1R activation may both diminish available PIP_2 stores leading to less IP_3 production and I_{CAN} desensitization, which would attenuate the inspiratory drive potential. This is consistent with attenuations observed in the amplitude of preBötC field recordings during applications of agonists for both $P2Y_1Rs$ and NK1Rs (Pena & Ramirez, 2004; Lorier *et al.* 2007).

TRPM4 and TRPM5 channels probably underlie I_{CAN} expressed by inspiratory neurons

We found mRNA coding for TRPM4 and TRPM5 channels in the preBötC region of the neonatal murine brainstem, despite previous reports that the brain is deficient in these genes (Perez *et al.* 2002; Nilius *et al.* 2003; Kunert-Keil *et al.* 2006). Our extraction methods provide a more sensitive test because we focused on a limited region of the ventral respiratory brain stem including the preBötC. Sampling the whole brain – even the whole brainstem – may dilute preBötC mRNA and thus increase the likelihood of a false negative.

Observing these genes in the preBötC is not sufficient to conclude that inspiratory neurons express functional TRPM4 and TRPM5 channels. Additionally, our protocol did not limit RNA extraction to preBötC inspiratory neurons but most probably sampled expiratory and non-respiratory neurons, as well as non-neural cells. It is also possible that post-transcriptional processing precludes the translation of one or both mRNAs. However, TRPM4 and TRPM5 are the only known channels that give rise to whole-cell currents with the biophysical properties of I_{CAN} present in preBötC neurons (Pace *et al.* 2007*a*) with respect to pharmacology, monovalent cation permeability and activation mechanism (Launay *et al.* 2002; Hofmann *et al.* 2003; Montell, 2005; Ullrich *et al.* 2005; Ramsey *et al.* 2006). While TRPM4 and TRPM5 differ in sensitivity to Ca^{2+} and FFA, fundamental properties of the two channels overlap substantially (Ullrich *et al.* 2005). We also documented that PIP_2 regulates I_{CAN}-dominated inspiratory drive potentials in a manner consistent with its effects on TRPM4 and TRPM5 channels. Therefore, we conclude that TRPM4 and TRPM5 channels are the ion channels underlying I_{CAN} in preBötC neurons.

Physiological role of PIP_2 in preBötC neurons

We propose that excess PIP_2 augments inspiratory drive potentials by counteracting I_{CAN} desensitization. Excess PIP_2 has no effect on non-desensitized TRPM5 channels (Liu & Liman, 2003) and pre-treatment with PIP_2

prevented TRPM4 desensitization from occurring (Nilius *et al.* 2006). Thus, PIP_2 counteracts desensitization but does not appear to augment other aspects of channel function. Our results with diC8-PIP_2 imply that I_{CAN} normally functions in a partially desensitized state in preBötC neurons during periodic respiratory activity.

TRPM4 and TRPM5 channels are mostly (or completely) deactivated at steady state when held at negative membrane potentials, which gives rise to their characteristic outwardly rectifying current–voltage curves (Hofmann *et al.* 2003; Liu & Liman, 2003; Nilius *et al.* 2003; Ullrich *et al.* 2005). PIP_2 reverses this desensitization for TRPM4 such that large inward currents gated by Ca^{2+} can flow at hyperpolarized membrane potentials (Nilius *et al.* 2006), and the same may be true for TRPM5 although the mechanism has not been fully documented (Liu & Liman, 2003). We propose that PIP_2 plays a similar role in preBötC neurons by alleviating (at least in part) I_{CAN} desensitization thus promoting its activation at negative voltages. This would enable I_{CAN} to participate to a greater extent in inspiratory burst generation, because inspiratory bursts initiate from baseline membrane potentials in the range –70 to –50 mV.

Consistent with this mechanism, diC8-PIP_2 frequently (4 cells out of 6 tested with diC8-PIP_2 and no Mg-ATP) augmented drive potentials at the onset of inspiratory bursts (see Fig. 3*D*). This suggests that bursts initiate at lower voltages (and possibly with smaller excitatory postsynaptic potentials as well) in the presence of excess PIP_2. Also supporting this interpretation, diC8-PIP_2 enabled small ectopic depolarizations to reach burst threshold (see Fig. 3*Fa* and *b*) and cause full-fledged inspiratory-like bursts. We conclude that the addition of exogenous PIP_2 augments inspiratory drive potential generation by lowering or removing the threshold of excitatory input necessary to activate I_{CAN}.

How might PIP_2-regulated I_{CAN} desensitization operate on a cycle-to-cycle basis to shape inspiratory bursts? If periodic PIP_2 depletion is involved in burst termination, then excess exogenous PIP_2 should stave off desensitization and delay inspiratory burst termination. However, this effect was only observed in 2 of the 6 neurons treated with diC8-PIP_2 (see Fig. 3*E*). We conclude that PIP_2 depletion (during IP_3 production) is not a major factor that governs inspiratory burst termination.

I_{CAN} in preBötC neurons normally functions in a partially desensitized state during rhythmic activity *in vitro*. Moreover, PIP_2 does not act on a cycle-to-cycle basis to cause burst termination nor promote burst onset. These two points are not in conflict; we theorize that PIP_2 maintains I_{CAN} functionality for the 'long haul', i.e. respiratory oscillations are meant to continue without lapse, conferring stability and longevity to inspiratory burst generation in a critical physiological system that necessitates both.

References

Balla T (1998). Phosphatidylinositol 4-kinases. *Biochim Biophys Acta* **1436**, 69–85.

Bartos M, Vida I & Jonas P (2007). Synaptic mechanisms of synchronized gamma oscillations in inhibitory interneuron networks. *Nat Rev Neurosci* **8**, 45–56.

Buzsáki G (2006). *Rhythms of the Brain*. Oxford University Press, Oxford, New York.

Clapham DE (2003). TRP channels as cellular sensors. *Nature* **426**, 517–524.

Enklaar T, Esswein M, Oswald M, Hilbert K, Winterpacht A, Higgins M, Zabel B & Prawitt D (2000). Mtr1, a novel biallelically expressed gene in the center of the mouse distal chromosome 7 imprinting cluster, is a member of the Trp gene family. *Genomics* **67**, 179–187.

Feldman JL & Del Negro CA (2006). Looking for inspiration: new perspectives on respiratory rhythm. *Nat Rev Neurosci* **7**, 232–242.

Gafni J, Munsch JA, Lam TH, Catlin MC, Costa LG, Molinski TF & Pessah IN (1997). Xestospongins: potent membrane permeable blockers of the inositol 1,4,5-trisphosphate receptor. *Neuron* **19**, 723–733.

Gray PA, Rekling JC, Bocchiaro CM & Feldman JL (1999). Modulation of respiratory frequency by peptidergic input to rhythmogenic neurons in the preBotzinger complex. *Science* **286**, 1566–1568.

Greenwood IA & Large WA (1995). Comparison of the effects of fenamates on Ca-activated chloride and potassium currents in rabbit portal vein smooth muscle cells. *Br J Pharmacol* **116**, 2939–2948.

Grillner S (2003). The motor infrastructure: from ion channels to neuronal networks. *Nat Rev Neurosci* **4**, 573–586.

Grillner S (2006). Biological pattern generation: the cellular and computational logic of networks in motion. *Neuron* **52**, 751–766.

Guinamard R, Chatelier A, Demion M, Potreau D, Patri S, Rahmati M & Bois P (2004*a*). Functional characterization of a Ca^{2+}-activated non-selective cation channel in human atrial cardiomyocytes. *J Physiol* **558**, 75–83.

Guinamard R, Chatelier A, Lenfant J & Bois P (2004*b*). Activation of the Ca^{2+}-activated nonselective cation channel by diacylglycerol analogues in rat cardiomyocytes. *J Cardiovasc Electrophysiol* **15**, 342–348.

Harks EG, de Roos AD, Peters PH, de Haan LH, Brouwer A, Ypey DL, van Zoelen EJ & Theuvenet AP (2001). Fenamates: a novel class of reversible gap junction blockers. *J Pharmacol Exp Ther* **298**, 1033–1041.

Hille B (2001). *Ion Channels of Excitable Membranes*, 3rd edn. Sinauer Associates, Sunderland, MA.

Hofmann T, Chubanov V, Gudermann T & Montell C (2003). TRPM5 is a voltage-modulated and Ca^{2+}-activated monovalent selective cation channel. *Curr Biol* **13**, 1153–1158.

Inoue S & Spring KR (1997). *Video Microscopy: the Fundamentals*. Plenum Press, New York.

Janczewski WA & Feldman JL (2006). Distinct rhythm generators for inspiration and expiration in the juvenile rat. *J Physiol* **570**, 407–420.

Kunert-Keil C, Bisping F, Kruger J & Brinkmeier H (2006). Tissue-specific expression of TRP channel genes in the mouse and its variation in three different mouse strains. *BMC Genomics* **7**, 159.

Launay P, Fleig A, Perraud AL, Scharenberg AM, Penner R & Kinet JP (2002). TRPM4 is a Ca^{2+}-activated nonselective cation channel mediating cell membrane depolarization. *Cell* **109**, 397–407.

Li H, Leeman SE, Slack BE, Hauser G, Saltsman WS, Krause JE, Blusztajn JK & Boyd ND (1997). A substance P (neurokinin-1) receptor mutant carboxyl-terminally truncated to resemble a naturally occurring receptor isoform displays enhanced responsiveness and resistance to desensitization. *Proc Natl Acad Sci U S A* **94**, 9475–9480.

Liu D & Liman ER (2003). Intracellular Ca^{2+} and the phospholipid PIP2 regulate the taste transduction ion channel TRPM5. *Proc Natl Acad Sci U S A* **100**, 15160–15165.

Lorier AR, Huxtable AG, Robinson DM, Lipski J, Housley GD & Funk GD (2007). P2Y1 receptor modulation of the pre-Botzinger complex inspiratory rhythm generating network in vitro. *J Neurosci* **27**, 993–1005.

Minke B (1977). Drosophila mutant with a transducer defect. *Biophys Struct Mech* **3**, 59–64.

Mironov SL, Langohr K & Richter DW (2000). Hyperpolarization-activated current, Ih, in inspiratory brainstem neurons and its inhibition by hypoxia. *Eur J Neurosci* **12**, 520–526.

Montell C (2005). The TRP superfamily of cation channels. *Sci STKE* **272**, re3.

Nakanishi S, Catt KJ & Balla T (1995). A wortmannin-sensitive phosphatidylinositol 4-kinase that regulates hormone-sensitive pools of inositolphospholipids. *Proc Natl Acad Sci U S A* **92**, 5317–5321.

Nilius B, Mahieu F, Prenen J, Janssens A, Owsianik G, Vennekens R & Voets T (2006). The Ca^{2+}-activated cation channel TRPM4 is regulated by phosphatidylinositol 4,5-biphosphate. *EMBO J* **25**, 467–478.

Nilius B, Prenen J, Droogmans G, Voets T, Vennekens R, Freichel M, Wissenbach U & Flockerzi V (2003). Voltage dependence of the Ca^{2+}-activated cation channel TRPM4. *J Biol Chem* **278**, 30813–30820.

Nilius B, Prenen J, Janssens A, Voets T & Droogmans G (2004). Decavanadate modulates gating of TRPM4 cation channels. *J Physiol* **560**, 753–765.

Nilius B, Prenen J, Tang J, Wang C, Owsianik G, Janssens A, Voets T & Zhu MX (2005). Regulation of the Ca^{2+} sensitivity of the nonselective cation channel TRPM4. *J Biol Chem* **280**, 6423–6433.

North RA & Barnard EA (1997). Nucleotide receptors. *Curr Opin Neurobiol* **7**, 346–357.

Ottolia M & Toro L (1994). Potentiation of large conductance KCa channels by niflumic, flufenamic, and mefenamic acids. *Biophys J* **67**, 2272–2279.

Pace RW, Mackay DD, Feldman JL & Del Negro CA (2007*a*). Inspiratory bursts in the preBötzinger complex depend on a calcium-activated non-specific cationic current linked to glutamate receptors in neonatal mice. *J Physiol* **582**, 113–125.

Pace RW, Mackay DD, Feldman JL & Del Negro CA (2007*b*). Role of persistent sodium current in mouse preBotzinger complex neurons and respiratory rhythm generation. *J Physiol* **580**, 485–496.

Paulsen M, El-Maarri O, Engemann S, Strodicke M, Franck O, Davies K, Reinhardt R, Reik W & Walter J (2000). Sequence conservation and variability of imprinting in the Beckwith–Wiedemann syndrome gene cluster in human and mouse. *Hum Mol Genet* **9**, 1829–1841.

Pena F & Ramirez JM (2004). Substance P-mediated modulation of pacemaker properties in the mammalian respiratory network. *J Neurosci* **24**, 7549–7556.

Perez CA, Huang L, Rong M, Kozak JA, Preuss AK, Zhang H, Max M & Margolskee RF (2002). A transient receptor potential channel expressed in taste receptor cells. *Nat Neurosci* **5**, 1169–1176.

Pierrefiche O, Champagnat J & Richter DW (1995). Calcium-dependent conductances control neurones involved in termination of inspiration in cats. *Neurosci Lett* **184**, 101–104.

Ramsey IS, Delling M & Clapham DE (2006). An introduction to trp channels. *Annu Rev Physiol* **68**, 619–647.

Rekling JC & Feldman JL (1998). PreBötzinger complex and pacemaker neurons: hypothesized site and kernel for respiratory rhythm generation. *Annu Rev Physiol* **60**, 385–405.

Richter DW, Champagnat J, Jacquin T & Benacka R (1993). Calcium currents and calcium-dependent potassium currents in mammalian medullary respiratory neurones. *J Physiol* **470**, 23–33.

Rohacs T, Lopes CM, Michailidis I & Logothetis DE (2005). PI (4,5),P_2 regulates the activation and desensitization of TRPM8 channels through the TRP domain. *Nat Neurosci* **8**, 626–634.

Roush ED & Kwatra MM (1998). Human substance P receptor expressed in Chinese hamster ovary cells directly activates $G_{\alpha q/11}$, $G_{\alpha s}$, $G_{\alpha o}$. *FEBS Lett* **428**, 291–294.

Ruangkittisakul A, Schwarzacher SW, Secchia L, Poon BY, Ma Y, Funk GD & Ballanyi K (2006). High sensitivity to neuromodulator-activated signaling pathways at physiological $[K^+]$ of confocally imaged respiratory center neurons in on-line-calibrated newborn rat brainstem slices. *J Neurosci* **26**, 11870–11880.

Runnels LW, Yue L & Clapham DE (2002). The TRPM7 channel is inactivated by PIP_2 hydrolysis. *Nat Cell Biol* **4**, 329–336.

Smith JC, Ellenberger HH, Ballanyi K, Richter DW & Feldman JL (1991). Pre-Bötzinger complex: a brainstem region that may generate respiratory rhythm in mammals. *Science* **254**, 726–729.

Srinivas M & Spray DC (2003). Closure of gap junction channels by arylaminobenzoates. *Mol Pharmacol* **63**, 1389–1397.

Suh BC & Hille B (2005). Regulation of ion channels by phosphatidylinositol 4,5-bisphosphate. *Curr Opin Neurobiol* **15**, 370–378.

Teulon J (2000). Ca^{2+}-activated nonselective cation channels. In *Pharmacology of Ionic Channel Function: Activators and Inhibitors*, ed.Endo M, Kurachi Y & Mishina M, pp. 625–649. Springer-Verlag, Berlin.

Thoby-Brisson M, Telgkamp P & Ramirez JM (2000). The role of the hyperpolarization-activated current in modulating rhythmic activity in the isolated respiratory network of mice. *J Neurosci* **20**, 2994–3005.

Ullrich ND, Voets T, Prenen J, Vennekens R, Talavera K, Droogmans G & Nilius B (2005). Comparison of functional properties of the Ca^{2+}-activated cation channels TRPM4 and TRPM5 from mice. *Cell Calcium* **37**, 267–278.

Wang D, Grillner S & Wallen P (2006). Effects of flufenamic acid on fictive locomotion, plateau potentials, calcium channels and NMDA receptors in the lamprey spinal cord. *Neuropharmacology* **51**, 1038–1046.

Wang H, Stornetta RL, Rosin DL & Guyenet PG (2001). Neurokinin-1 receptor-immunoreactive neurons of the ventral respiratory group in the rat. *J Comp Neurol* **434**, 128–146.

Zhang H, Xu Y, Zhang Z, Liman ER & Prestwich GD (2006). Synthesis and biological activity of phospholipase C-resistant analogues of phosphatidylinositol 4,5-bisphosphate. *J Am Chem Soc* **128**, 5642–5643.

Zhang Z, Okawa H, Wang Y & Liman ER (2005). Phosphatidylinositol 4,5-bisphosphate rescues TRPM4 channels from desensitization. *J Biol Chem* **280**, 39185–39192.

Zolles G, Klocker N, Wenzel D, Weisser-Thomas J, Fleischmann BK, Roeper J & Fakler B (2006). Pacemaking by HCN channels requires interaction with phosphoinositides. *Neuron* **52**, 1027–1036.

Acknowledgements

This work was supported by National Science Foundation IOB-0616099 (USA), the Suzann Wilson Matthews Faculty Research Award (The College of William and Mary, Williamsburg, VA, USA), the Jeffress Memorial Trust (Richmond, VA, USA), and grants in support of undergraduate research from the Howard Hughes Medical Institute Undergraduate Science Education Grant awarded to The College of William and Mary (M. S. Saha, Project director). G.D.P. thanks the NIH for NS29632 and W. Huang (University of Utah) for molecular simulations.

Supplemental material

Online supplemental material for this paper can be accessed at:

http://jp.physoc.org/cgi/content/full/jphysiol.2007.134577/DC1

and

http://www.blackwell-synergy.com/doi/suppl/10.1113/jphysiol.2007.134577